

Investigation of the In-Gap Electronic Structure of LaAlO₃ - SrTiO₃ Heterointerfaces by Soft X-ray Spectroscopy

A. Koitzsch¹, J. Ocker¹, M. Knupfer¹, M. C. Dekker¹, K. Dörr¹, B. Büchner¹, and P. Hoffmann²

¹*Institute for Solid State Research, IFW-Dresden, P.O.Box 270116, D-01171 Dresden, Germany*

²*Helmholtz-Zentrum Berlin, BESSY, Albert-Einstein-Str. 15, D-12489 Berlin, Germany*

(Dated: April 27, 2022)

We investigated LaAlO₃ - SrTiO₃ heterointerfaces grown either in oxygen rich or poor atmosphere by soft x-ray spectroscopy. Resonant photoemission across the Ti L_{2,3} absorption edge of the valence band and Ti 2p core level spectroscopy directly monitor the impact of oxygen treatment upon the electronic structure. Two types of Ti³⁺ related charge carriers are identified. One is located at the Fermi energy and related to the filling of the SrTiO₃ conduction band. It appears for low oxygen pressure only. The other one is centered at $E_B \approx 1$ eV and independent of the oxygen pressure during growth. It is probably due to defects. The magnitude of both excitations is comparable. It is shown that low oxygen pressure is detrimental for the Ti - O bonding. Our results shed light on the nature of the charge carriers in the vicinity of the LaAlO₃ - SrTiO₃ interface.

I. INTRODUCTION

Fascinating and counterintuitive phenomena have been observed at the interface of SrTiO₃ and LaAlO₃. The most important is the appearance of metallic conductivity between two firm insulators¹. Intriguingly the interface remains insulating as long as no more than three layers of LaAlO₃ are deposited on top of SrTiO₃ but switches to metallic with the fourth layer^{2,3}. Subsequently, also superconductivity was found below $T_C = 0.2$ K⁴ and even magnetism⁵. The picture of the polar catastrophe has been invoked early on to explain the metallic conductivity: stacking of LaO⁺ and AlO₂⁻ layer by layer on top of SrTiO₃ leads to a divergent electrostatic potential which is compensated by a charge transfer of 0.5 e⁻ per unit cell to the interface for the case of LaO deposited on TiO₂. These charge carriers are hold responsible for metallicity at the interface.

The polar catastrophe is conceptually simple and explains elegantly the change of groundstates for three vs four layers of LaAlO₃. However, experimental evidence for the importance of oxygen vacancies as effective doping mechanism has been presented^{6,7}. In fact the observed sheet carrier density for heterostructures grown in oxygen poor atmosphere ($p_{O_2} = 10^{-6}$ mbar) assumes values several orders of magnitudes larger than what is expected at maximum for e/2 charge transfer for the polar catastrophe. On the other hand, for samples grown under higher oxygen partial pressure the charge density significantly decreases. These observations support the view that oxygen vacancies are essential for the properties of the interface. Depending on growth conditions they may completely dominate the low energy properties or - at least - compete with the polar catastrophe. A third important concept for the description of the LaAlO₃ - SrTiO₃ heterostructure is intermixing of the chemical species, which tends to mitigate polar discontinuities or to invoke a (La, Sr)TiO₃ layer at the interface⁸⁻¹¹.

Photoemission spectroscopy is sensitive to all of these three mechanisms, polar catastrophe, oxygen vacancies

and intermixing, and has been applied previously to the LaAlO₃ - SrTiO₃ system. Segal et al. did not observe the consequences of strong internal fields connected to the LaAlO₃ layer such as line broadening and shifting¹². Metallic charge carriers arising from electronic reconstruction or oxygen vacancies form a Fermi edge in photoemission experiments as soon as their concentration is detectable. For the LaAlO₃ - SrTiO₃ system the intensity at E_F has been studied as a function of p_{O_2} and found to decrease with p_{O_2} increase for standard ultraviolet photoemission¹³. Interestingly, no Fermi edge signal and no other in gap states were found for Molecular Beam Epitaxy (MBE) grown metallic samples even for the Ti L resonance (which is known to greatly enhance the Ti 3d derived density of states) from which upper limits for the charge concentration were deduced¹⁴. In contrast, a recent study on pulsed laser deposition (PLD) - grown samples did find in-gap states reaching up to E_F , whose intensity depends on the number of LaAlO₃ layers¹⁵. Cation intermixing has been studied by monitoring the intensity profiles of suitable core levels excitations as a function of emission angle^{10,16}. These profiles are inconsistent with an abrupt interface.

It is fair to say that no coherent picture for the spectroscopic investigations of the LaAlO₃ - SrTiO₃ system has emerged yet. Here we study the in-gap states with particular attention to the influence of the oxygen pressure during growth. The latter is apparently a decisive parameter for the LaAlO₃ - SrTiO₃ heterostructures and has a direct and well documented impact on the transport properties, e.g. it tunes the electrical conductivity over many orders of magnitude. We consider two limiting cases: samples grown under low ($4.5 \cdot 10^{-6}$ mbar) and high ($5 \cdot 10^{-3}$ mbar) oxygen atmosphere. The goal of this study is to monitor the effect of the latter on the electronic structure. To this end we recorded detailed photoemission spectra of the valence band and Ti-states.

The paper is structured as follows: In section II the experimental procedures are described as well as sample preparation and characterization. Section III presents the results from valence band PES and from the core

levels. In section IV the results are discussed.

II. EXPERIMENTAL

Experiments have been carried out at the Helmholtz Zentrum Berlin (BESSY) at undulator beamline UE 52. Photoemission measurements have been performed using a Scienta R4000 photoelectron analyzer. The total energy resolution has been set to 260 meV for 440 eV photon energy and 620 meV for 1200 eV. X-ray absorption has been measured by monitoring the drain current.

LaAlO₃ - SrTiO₃ heterostructures with an conducting LaO - TiO₂ interface were fabricated on atomically flat TiO₂ terminated SrTiO₃ single crystals by pulsed laser deposition. In order to obtain TiO₂ terminated SrTiO₃ substrates a cleaning and BHF etching procedure was applied¹⁷. The SrTiO₃ single crystal, dried with argon gas was annealed at 950 °C in oxygen atmosphere for 3 hours, in order to recrystallize the substrate, hence forming atomically flat parallel terraces. During growth the thickness of each LaAlO₃ layer was controlled on an atomic scale by monitoring the intensity oscillations of the specular spot in reflection high-energy electron diffraction (RHEED). The samples were grown at 800 °C with a laser fluence of 2-3 J/cm², resulting in growth of approximately 0.7 Å per pulse. No further oxidation step was performed after the deposition process. Sample OR (oxygen rich) was grown at $5.0 \cdot 10^{-3}$ mbar oxygen pressure and the thickness was fixed to 5 unit cells LaAlO₃, whereas sample OP (oxygen poor) was grown at $4.5 \cdot 10^{-6}$ mbar with 6 unit cells. The samples have been cleaned by acetone rinsing before transfer to the UHV system. No further in situ cleaning procedure was applied before measurements.

The surface morphology of the heterostructures has been determined by atomic force microscopy. The step- and terrace structure of the substrate is preserved throughout the growth of the LaAlO₃ film for low and high oxygen partial pressures. For sample OP the LaAlO₃ surface is smooth and does not show any variations in microstructure. Sample OR grown in higher oxygen pressure shows small islands of LaAlO₃ at the step edges. The islands are 1 unit cell high and appear independently of the growth temperature.

The conductivity of the samples has been checked in dependence on temperature using wire-bonded Al contacts. Fig. 1 shows the sheet resistance of the oxygen-poor (OP) sample which is metallic with a residual resistance ratio of $R_{sheet}(300\text{ K})/R_{sheet}(10\text{ K}) = 174$. The magnitudes of R_{sheet} and the resistance ratio fit well into the resistance characteristics recorded for various deposition pressures in Ref. 5, considering the pressure of $4.5 \cdot 10^{-6}$ mbar for the OP sample. The oxygen-rich (OR) sample proved to have a high sheet resistance with $R_{sheet} > 10^6 \Omega$ in the entire temperature range of 10 - 300 K, exceeding the range of measurable resistances of our setup.

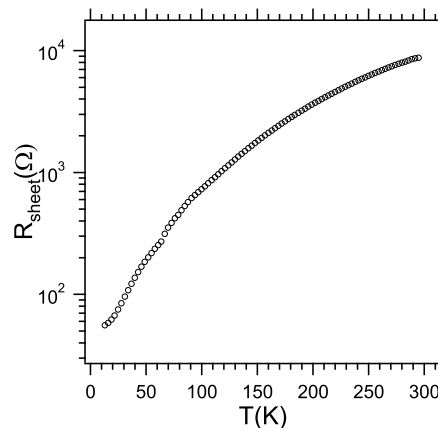


FIG. 1. Sheet resistance of sample OP (grown in oxygen poor atmosphere).

III. RESULTS

A. Valence Band

To unravel the origin of metallic conductivity of the LaAlO₃ - SrTiO₃ interface it is essential to investigate the electronic states at and near the Fermi energy. We start the presentation of the experimental results with valence band data of sample OP in Fig. 2. Fig. 2a shows the valence band as a function of photon energy across the Ti L_{2,3} absorption edge over a wide binding energy range capturing the shallow core levels which have been used for normalization. The Fermi energy (E_F) has been obtained by referencing to the Fermi edge of gold in electrical contact to the sample. However, small changes (in the order of 0.1 eV) occurred for the different photon energies across the edge energies, possibly related to residual charging. Therefore, we will not discuss absolute binding energies with this precision. In general the observed valence bands are a mixture of contributions from SrTiO₃ and LaAlO₃. However, near E_F only SrTiO₃ states are present. The band gap of pure SrTiO₃ is 3.2 eV at room temperature and the conduction band minimum is located at 0.2-0.3 eV above E_F ¹⁸. With n-type doping the conduction band is occupied and the onset of the valence band shifts to higher binding energy. LaAlO₃, on the other hand, has a larger band gap (5.6 eV). Conduction band minimum and valence band maximum of LaAlO₃ are each approximately 3 eV away from E_F , thus the close vicinity of E_F is solely determined by SrTiO₃ states.

The bottom spectrum in Fig. 2a has been taken well before the onset of the Ti L_{2,3} absorption edge, i.e. off-resonant. For this off-resonant spectrum no Fermi edge is visible and no signature of in-gap states frequently observed for SrTiO₃ and other Ti⁴⁺ systems¹⁸⁻²⁴. The main valence band ($E_B = 3 - 9$ eV) is composed of a high and low binding energy region (V_1 and V_2). At higher binding energies shoulder structures (C and L) appear.

Feature C at 11 eV is probably related to surface adsorbates, which are notorious in this energy region. The energy position of feature L coincides with a structure in the LaAlO₃ valence band.

The photon energy has been swept through the Ti L_{2,3} absorption edge shown in Fig. 2c. The shape of the absorption spectra compares favorably with the result of a multiplet calculation for Ti⁴⁺. The four prominent peaks of this spectrum correspond to the spin-orbit splitting of the Ti 2p level and the crystal field splitting in t_{2g} and e_g states for each of the spin-orbit components. In comparison, the Ti³⁺ spectrum looks very different and can be easily distinguished (Fig. 2c, inset). It is well known that the resonance photoemission process enhances the Ti 3d related density of states in the valence band. For a Ti⁴⁺ system the Ti 3d bands are nominally empty, thus any resonance enhancement is a signature of Ti 3d - O 2p hybridization.

As the photon energy is tuned through the Ti L edge intensity enhancements occur in the valence band. We distinguish three characteristic regions: the low energy region near E_F (see expanded view in Fig. 2b), the enhancement of the main valence band (V₁ and V₂) and weak but discernible increase at higher binding energy around E_B = 12 - 15 eV (satellites S₁ and S₂). The strongest enhancement occurs for the high binding energy region of the valence band (feature V₂), which is much more enhanced than the low binding energy region (V₁). This is in agreement with previous studies and has been interpreted as a consequence of predominantly bonding O 2p orbitals at the high binding part of the valence band with relatively strong Ti 3d admixture, whereas the region V₂ is dominated by nonbonding O 2p orbitals with little Ti 3d overlap^{20,24,26}.

More interesting than the behavior of the main valence band is, however, the low energy region close to the Fermi energy. We observe clear intensity enhancement upon entering the resonance regime in the region of E_B = 0 - 2 eV. In Fig. 2b we show the difference spectra obtained by subtracting the off-resonant spectra. The line shape of the remaining difference spectra can be described by two components, one centered close to the Fermi energy (G₁), the other one centered around E_B = 1 eV (G₂). In particular feature G₁ is cut off by E_F signaling the metallic nature of these charge carriers. These observations are similar to previous results for SrTiO₃^{18,24} and SrTiO₃ heterostructures^{7,15,23}. Due to the low oxygen partial pressure during growth oxygen vacancies are expected to form in sample OP. Oxygen vacancies induce effective electron doping and create lattice defects. Feature G₁ is naturally explained by the filling of the bottom of the SrTiO₃ conduction band. The fact that it is visible on-resonant but not off-resonant shows that the bottom of the conduction band is predominantly of Ti 3d character. The relative intensity of G₁ and G₂ depends on the specific photon energy, G₁ resonating more strongly for e_g excitations. For SrTiO₃ this has been associated previously with the k_z dispersion of the crystalline material.

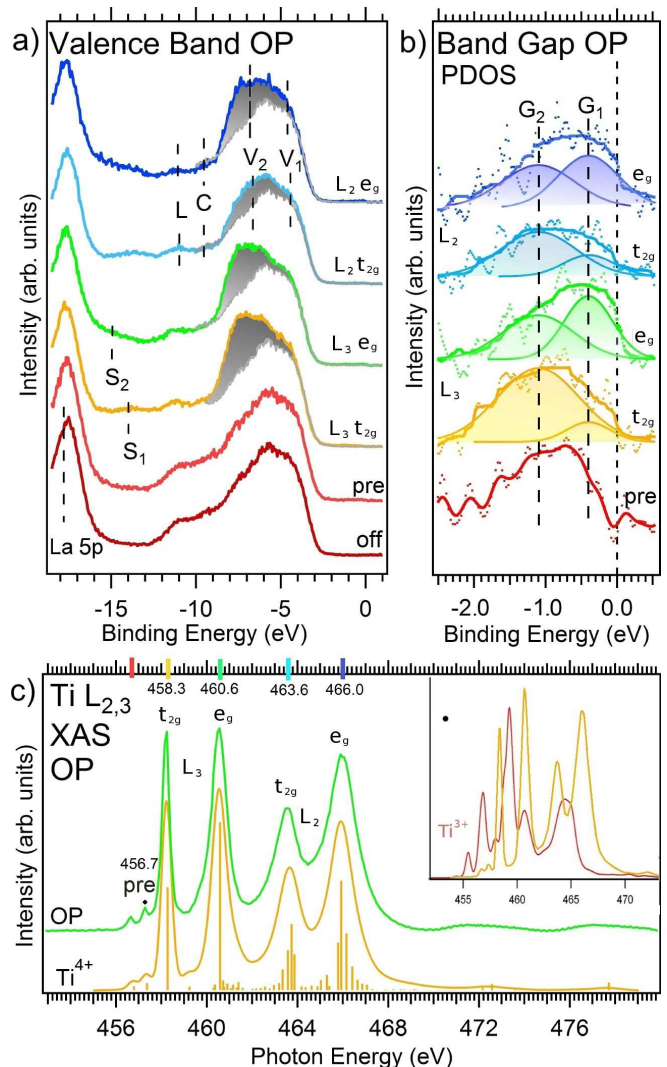


FIG. 2. (Color online) Valence band photoemission of LaAlO₃ - SrTiO₃ (sample OP, grown in oxygen poor atmosphere). a) Ti 2p → 3d resonant photoemission valence band obtained by varying the photon energy through the Ti L_{2,3} absorption threshold. The grey area shows the enhancement of Ti 3d derived states by comparison with the off-resonant spectrum at hν = 440 eV. b) Difference spectra near E_F obtained by subtracting the off resonant spectrum (hν = 440 eV) from the on - resonant spectra. Thick lines are obtained from the original data by moderate smoothing. c) Ti L_{2,3} absorption edge taken in total electron yield mode compared to a multiplet calculation²⁵. Color bars at the top indicate the photon energy of the valence band spectra. Inset shows a comparison of calculated L_{2,3} Ti⁴⁺ and Ti³⁺ absorption edges.

In particular, maxima of G₁ have been explained by the E_F crossing of an electron pocket²⁴. The shape of the low energy spectral weight and the dependence of G₁ on photon energy is very similar to n-doped SrTiO₃²⁴. The fact that strong resonance enhancement occurs already before the onset of the main Ti⁴⁺ absorption (spectrum "pre" in Fig. 2) is consistent with the in-gap states being of Ti³⁺ character because the Ti³⁺ absorption starts at

lower energy than Ti^{4+} (see inset Fig. 2c).

Finally, between 13 and 15 eV weak peaks appear on resonant (S_1 and S_2) depending on the intermediate state being of t_{2g} or e_g symmetry. S_2 is actually difficult to recognize in Fig. 2a, but becomes apparent when the difference spectra are considered (see Fig. 4). Ti - related intensity in this energy region has been assigned previously to a $3d^1L^2$ satellite state, where L refers to a ligand hole. Similar satellites are observed for the Ti 2p line as well²⁶. For clarity we postpone the discussion of the difference of S_1 and S_2 to Fig. 4.

In Fig. 3 we present equivalent results for sample OR which has been exposed to substantially enhanced oxygen concentration during the growth process ($p_{O_2} = 5 \cdot 10^{-3}$ mbar). This is supposed to reduce the formation of oxygen vacancies and hence of effective electron doping. The shape of the valence band is similar to sample OP and we apply the same notation scheme. In agreement with the high resistance of the sample, substantial charging related shifts have been observed. Therefore, the valence bands in Fig. 3 have been aligned to sample OP using the shallow core levels.²⁷ In contrast to OP there exists a low binding energy foot near E_F even for the off resonant case. When sweeping the photon energy through the Ti $L_{2,3}$ edge some enhancement occurs in that region, but no intensity is revealed at E_F (Fig. 3b). The Ti 3d related enhancement is centered at $E_B = 1$ eV which is at the same position as feature G_2 for sample OP. Hence, in contrast to OP, G_1 is absent and the density of states at E_F sharply reduced. This is consistent with a reduced n - doping of the sample due to the higher oxygen partial pressure. It is also consistent with the measured resistance.

Fig. 3c presents a comparison of the Ti $L_{2,3}$ absorption edges of samples OP and OR. The overall shape is similar, but OP has slightly broader peaks. The latter effect is more clearly seen for the Ti 2p photoemission measurements (Fig. 5) and naturally explained by increased disorder due to the larger density of oxygen vacancies. Also shown in Fig. 3c is the integrated intensity of the main valence band ($E_B = 3 - 9$ eV) as a function of photon energy (red asterisks). This follows the absorption spectra rather well, confirming the Ti^{4+} character of these states.

Apart from the Ti - related features G_1 and G_2 a foot structure appears around $E_B = 2$ eV for sample OR. Since this is observed off-resonant it must be O 2p related. The additional oxygen during growth of OR avoids formation of oxygen vacancies but may introduce new types of disorder. It may also cause a less coherent film growth.

Fig. 4 provides a direct comparison of the on-resonant valence bands of both samples. Spectra have been normalized at the O 2s peak and background corrected. Difference spectra (PDOS) have been rescaled to correct for the different numbers of LaAlO_3 layers²⁸. We start the discussion with the main valence band (features V_1 and V_2). The overall shape of the main valence band agrees

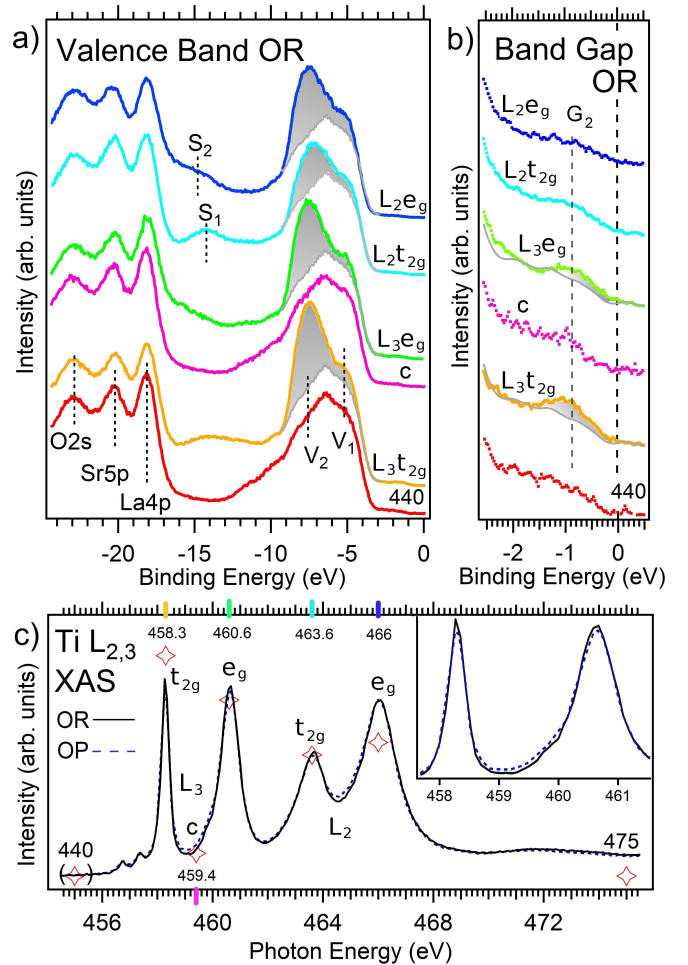


FIG. 3. (Color online) Valence band photoemission of $\text{LaAlO}_3 - \text{SrTiO}_3$ (sample OR, grown in oxygen rich atmosphere). a) Ti $2p \rightarrow 3d$ resonant photoemission valence band obtained by varying the photon energy through the Ti $L_{2,3}$ absorption threshold. The grey area shows the enhancement of Ti 3d derived states by comparison with off-resonant spectra at 440 eV. b) Expanded view on the spectra shown in (a) near E_F . Grey line corresponds to the off-resonant measurement. c) Ti $L_{2,3}$ absorption edges of samples OR and OP taken in total electron yield mode. Color bars indicate the photon energy for the valence band spectra. Red asterisks correspond to the integrated valence band between $E_B = 3$ and 9 eV for different photon energies (constant initial state scan - CIS). Inset: Expanded view on the first two peaks.

well with the calculated Ti 3d density of states (DOS) of SrTiO_3 shown at the bottom of Fig. 4a. Interestingly, the relative intensity of V_2 is reduced for sample OP compared to OR. OP is the sample with more oxygen vacancies and V_2 originates from bonding Ti 3d - O 2p states. This suggests, that the vacancies disturb the crystalline order and chemical bonding. Also the reduced intensity of sample OR directly at E_F becomes apparent. The intensity around $E_B = 1$ eV (corresponding to feature G_2 in Fig. 2 + 3) is larger for sample OR when normalized to the shallow core levels (Fig. 4b, upper

spectra) due to the additional foot structure which is absent for sample OP. The Ti 3d related intensity at $E_B = 1$ eV, however, is comparable for both samples indicating a similar concentration of Ti defects.

In Fig. 4a the different position of S_1 and S_2 for t_{2g} and e_g excitations is clearly visible. We have assigned these satellites to a $3d^1L^2$ configuration. However, the d - electron of this excited state may occupy t_{2g} or e_g levels, which differ in energy by the crystal field splitting. Indeed the energy difference between S_1 and S_2 agrees with the $t_{2g} - e_g$ distance obtained from the XAS peak distance. Moreover, the e_g - satellite should appear at higher binding energy than the t_{2g} - satellite, which is indeed the case.

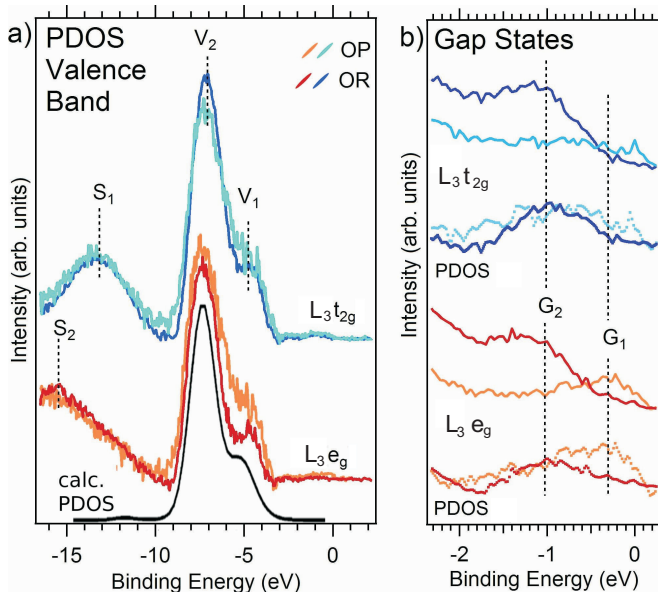


FIG. 4. (Color online) a) Resonance enhancement of the valence band for $h\nu = 458.3$ eV (t_{2g}) and 460.6 eV (e_g) for samples OP and OR. The calculated density of Ti 3d states is reproduced from Fujii et al.²⁹. Shown is the difference between on- and off-resonant. b) upper part (blue spectra): Comparison of low energy spectra (uppermost curves) and resonance enhancement (difference on-, off- resonant) for $h\nu = 458.3$ eV excitation energy (t_{2g}). Lower part (orange/red): The same for $h\nu = 460.6$ eV (e_g).

The description of the valence band data is consistent with the assumption, that the concentration of oxygen vacancies is considerably different in the samples and that these defects cause an electron doping of the sample.

B. Core Levels

The presence of charge carriers of Ti $3d^1$ character must also alter the shape of the Ti core levels for they effectively correspond to Ti^{3+} states, which differ in energy from the host Ti^{4+} environment. In particular Ti^{3+} shows up at the low energy side of the Ti 2p core level as has been quantitatively evaluated by Sing et al.³⁰.

TABLE I. Fit parameter for Fig. 5 .

Sample	FWHM $2p_{3/2}$	FWHM $2p_{1/2}$	$I(Ti^{3+})/I(Ti^{4+})$
OR 1220 eV	1.07	1.70	0.068 ± 0.019
OP 1210 eV	1.22	1.94	0.047 ± 0.04
OP 1500 eV	1.24	2.0	0.038 ± 0.017

In Fig. 5 we present Ti 2p spectra for both samples measured around 1200 eV and 1500 eV photon energy. A Shirley background has been subtracted from the raw data. For the OP 1210 eV spectrum the contribution of an Auger line has been subtracted out before the background subtraction³¹. The spectra have been aligned to the Ti $2p_{3/2}$ line. No reference is made to absolute binding energies due to obvious charging related shifts of sample OR and occasional residual shifts of sample OP.

For sample OP a low energy foot is discernible at the Ti $2p_{3/2}$ line, which is absent or much weaker for sample OR. Each spectrum has been fitted with two doublets of Voigt functions. The intensity ratio of the generic Ti^{4+} peaks has been fixed to 2 : 1, whereas the second, smaller component was allowed to vary freely. For all spectra the presence of the second component improves the fit significantly. The second component corresponds to Ti^{3+} states, which has been also observed in the valence band near E_F on resonance (see above). The intensity ratio of the Ti^{3+} doublet is close to 2 : 1 for OR but not for OP. For the 1210 eV OP spectra the $Ti^{3+} 2p_{1/2}$ peak shows an artificially broad and intense structure, which might be related to incomplete background removal. The $Ti^{3+} 2p_{1/2}$ component for OP 1500 eV, on the other hand, is rather sharp and has low intensity, possibly related to the signal to noise ratio at hand. Nevertheless, clear observations can be made from Fig. 5. For sample OP the energy position of the Ti^{3+} doublet is considerably shifted to lower energies with respect to OR. The absolute values of the $Ti^{3+} 2p_{3/2} - Ti^{4+} 2p_{3/2}$ energy separation for OP (ca. 2.0 eV) are close to previous reports for similar samples³⁰.

The appearance of two distinct Ti^{3+} states in the Ti 2p spectra is fully consistent with the observations from the valence band where also two Ti^{3+} components have been found. We associate the Ti^{3+} components of sample OP with structure G_1 ($SrTiO_3$ conduction band states) and Ti^{3+} of sample OR with G_2 . Since G_2 is present for both samples it contributes to the OP sample as well but is masked by G_1 . Only when G_1 is absent (sample OR) it can be resolved by fitting. The results of the fitting are summarized in table I. We use the Ti^{3+}/Ti^{4+} value for the following estimation of the charge carrier density near the interface.

The electron escape length λ of the Ti 2p photoelectrons for $h\nu = 1200$ eV in $LaAlO_3$ is calculated by using the TTP - 2M formalism to be 15.6 Å or approximately 4 unit cells³². By definition the majority of the photoemission signal originates from a layer of this thick-

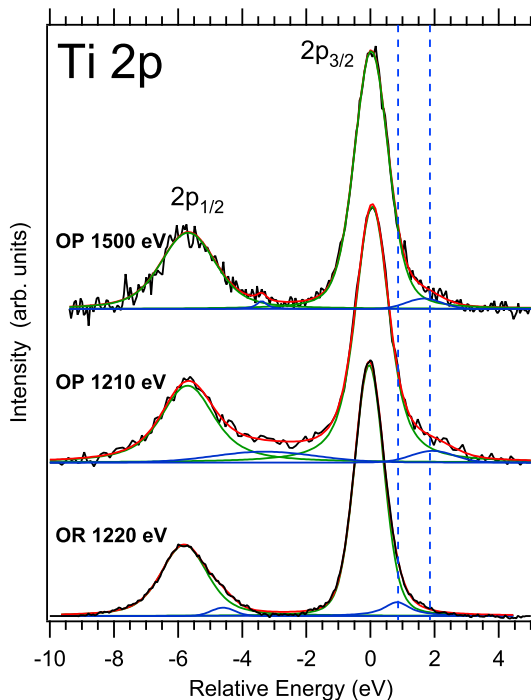


FIG. 5. (Color online) Ti 2p spectra measured in normal emission geometry fitted with Voigt functions (see text). Ti^{4+} peaks are shown in green, the smaller Ti^{3+} peaks in blue. The overall fit is red. Background has been removed before fitting. Vertical dashed lines highlight the positions of the low energy components.

ness. Note, that for the Ti 2p photoelectrons the LaAlO_3 overlayer acts as damping barrier, it does not change the $\text{Ti}^{3+}/\text{Ti}^{4+}$ ratio - provided Ti intermixing can be neglected. Assuming a constant Ti^{3+} distribution over λ , the charge carrier concentration for sample OP near the interface is appr. 4 - 5 %. The exact value depends on the total thickness of the Ti^{3+} layer d , which, unfortunately, cannot be obtained from the present experiment with sufficient accuracy. A lower limit of the sheet carrier density based on the above assumptions yields $n \approx 1.3 \cdot 10^{14} \text{ cm}^{-2}$. Note, that the true value could be substantially larger if $d \gg \lambda$.

The line widths of the Ti^{4+} peaks of sample OR are narrower than for sample OP (see Table 1). This is consistent with the Ti L absorption lines. It is probably related to increased overall disorder at the Ti - site in sample OP due to the higher density of oxygen vacancies with respect to OR.

Fig. 6 shows the O 1s lines for both samples. Whereas the Ti 2p measurement is mainly sensitive to the interface region, O 1s probes predominantly the LaAlO_3 surface. The line consists of two components: the main component at lower binding energy stemming from the LaAlO_3 lattice, and the contamination shoulder at higher binding energies, probably related to hydroxylation³³. It has been pointed out recently that adsorbates at the polar LaAlO_3 surface may alter the interface properties by

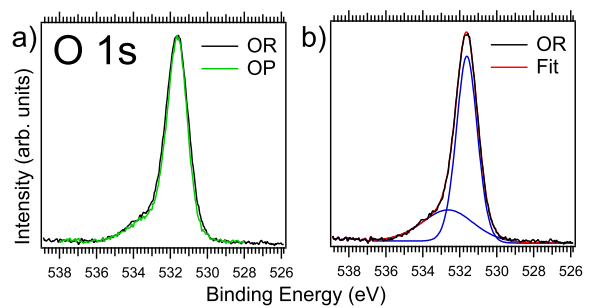


FIG. 6. (Color online) O 1s spectra measured in normal emission geometry with $h\nu = 1200 \text{ eV}$.

modifying the electrostatic potential across the LaAlO_3 overlayer³⁴. In this respect it is important to check whether the surfaces of our two samples look substantially different concerning the adsorbates. As can be seen in Fig. 6a this is not the case. The spectra are almost identical. This rules out the possibility that the observed differences among the samples arise from different surface characteristics. The intensity of the contamination peak is $\sim 30 \%$, similar to previous reports³⁵.

IV. DISCUSSION

The oxygen treatment has apparent consequences for the electronic structure of the LaAlO_3 - SrTiO_3 interface. We focus the discussion on the in-gap features as they determine the transport properties. We have identified three types of in-gap states: G_1 , G_2 and the foot structure at the valence band onset of sample OR. G_1 and G_2 are related to $\text{Ti } 3d^1$ as they resonate across the Ti L edge. They are ubiquitous for SrTiO_3 and related systems and have been observed for thin films²⁴ and, similarly, single crystals²². Their origin is at the center of a longstanding and, so far, not completely resolved debate. The most widespread interpretation is in terms of oxygen vacancy related defects. The feature near $E_B = 1 \text{ eV}$ is then due to $\text{Ti } 3d$ - O-vacancy complexes where an additional electron is trapped and forms a localized state. In contrast, the states at E_F are formed by electrons injected into the SrTiO_3 conduction band. But if only oxygen vacancies were decisive for the formation of feature G_2 one would expect some dependence of its intensity on oxygen pressure during growth. From the direct comparison in Fig. 4, however, G_2 is of similar intensity among the samples, or even more pronounced for sample OR. Therefore, a scenario where G_2 depends on the oxygen vacancy density alone seems inappropriate. Rather one has to consider defects arising from other types of local chemical disorder.

Another difference between the samples is the appearance of the foot structure of sample OR. It is apparently not related to $\text{Ti } 3d$ orbitals but rather to oxygen orbitals. If one recalls, that sample OR has been grown in rela-

tively high oxygen pressure compared to sample OP, it is tempting to associate the additional intensity with some additional or disordered oxygen in the lattice. However, the perovskite lattice is not susceptible to, e.g. oxygen interstitials. Rather this feature could be related to a less coherent film growth under higher oxygen pressure.

Coming back to the origin of G_2 , an often discussed possibility in this regard concerns the cations, La and Sr. It was observed early on that Ar - sputtering of SrTiO_3 surfaces does not only create oxygen vacancies but also strontium vacancies¹⁸. The PLD process relies on a non-equilibrium ion bombardment of the substrate, which, moreover, has been treated beforehand by an aggressive chemical procedure. Therefore, Sr-vacancies could play a role for SrTiO_3 . Furthermore, the deposition of the LaAlO_3 layers is known to introduce partial intermixing across the interface, as has been observed previously by several groups^{6,8,10}. This means that Sr diffuses into the LaAlO_3 layer and La into SrTiO_3 . However, it has been also reported that the intermixing depends on the oxygen pressure as well³⁶. This can be understood by deceleration and thermalization of the incoming ions by the more dense oxygen atmosphere. This would imply a dependence of G_2 on the oxygen pressure during growth. Nevertheless, the occurrence of such defects is related to the PLD process and cannot be ruled out.

We mention that alternative interpretations of G_2 have been proposed, i.e. such that do not involve defects. In the limit of high doping levels the system approaches a $3d^1$ configuration, which results in a Mott insulating state, as is realized e.g. in LaTiO_3 ³⁷. It is clear that the spectral function has to undergo drastic changes in this process. In this respect G_2 could be associated with a precursor of the lower Hubbard band. In fact the in-gap states of LaTiO_3 - SrTiO_3 interfaces have been studied by Takizawa et al. by off- and on-resonant photoemission and found to be consistent with such an interpretation²³. However, the doping levels for our samples, especially OR, are too small to sustain this scenario.

Ishida et al.²⁴ assigned the in-gap state at $E_B = 1.5$ eV in Nb-doped SrTiO_3 to a local screening channel of the d - orbitals. However, in our case the potential well screened state at E_F is virtually absent for sample OR, rendering this scenario for our situation unlikely as well.

From our point of view a defect related origin of the G_2 peak remains as the most plausible possibility. But it is not easy to clarify its exact nature. This issue clearly requires further investigations.

We now turn to another open question. Within the

picture of the polar catastrophe charge carriers should be present at the interface of sample OR, but are, within the sensitivity of our experiments, not observed. The resistance is too high and no intensity is measured at E_F . Why is this so? We propose a scenario where the G_2 defects (which are of substantial $\text{Ti } 3d^1$ character) cause a localization of electrons and deprive thereby the interface of itinerant charge carriers. The additional charge transferred to the interface by the polar catastrophe reconstruction maybe lost in this way for electrical conductivity, although it still balances the electrostatics at the interface and may give rise to localized magnetic moments⁵. For sample OP there are enough oxygen vacancy related additional electrons to compensate this and still populate the conduction band, but not for sample OR. In fact the defect density is high enough to support this scenario: i) From the direct comparison in Fig. 4 and from the fitting results of the $\text{Ti } 2p$ lines the conclusion is justified, that G_1 and G_2 have roughly the same intensity, i.e. considering the reasonable transport properties of OP, the defect density must be substantial. ii) From the Ti^{3+} component of the OR - $\text{Ti } 2p$ line a minimal sheet defect density of $\sim 2 \cdot 10^{-14} \text{ cm}^{-2}$ near the interface can be estimated (table I). This could be enough to outweigh the effect of the polar catastrophe with an upper limit of the sheet carrier density of $3.4 \cdot 10^{-14} \text{ cm}^{-2}$.

Alternatively, the polar discontinuity maybe mitigated by cationic displacement and intermixing from the beginning, leaving the presence of oxygen vacancies as the only source of charge carriers .

V. SUMMARY

We have investigated the LaAlO_3 - SrTiO_3 heterointerface by soft x-ray spectroscopy for different sample treatments. The population of the SrTiO_3 conduction band is directly seen for the sample grown in low oxygen atmosphere but is absent for the sample grown in high oxygen atmosphere. Another prominent Ti - related state is observed within the SrTiO_3 gap and is probably related to disorder induced defects. Both types of Ti^{3+} related states - conduction electrons and defects - are visible near the Fermi energy but also at the low energy side of the $\text{Ti } 2p$ core level. The results signal a varying charge carrier concentration among the samples, likely caused by a growth dependent defect density.

¹ A. Ohtomo and H. Hwang, *Nature*, **427**, 423 (2004).

² S. Thiel, G. Hammerl, A. Schmehl, C. W. Schneider, and J. Mannhart, *Science*, **313**, 1942 (2006).

³ M. Huijben, G. Rijnders, D. Blank, S. Bals, S. Van Aert, J. Verbeeck, G. Van Tendeloo, A. Brinkman, and H. Hilgenkamp, *Nature Materials*, **5**, 556 (2006).

⁴ N. Reyren, S. Thiel, A. D. Caviglia, L. F. Kourkoutis, G. Hammerl, C. Richter, C. W. Schneider, T. Kopp, A.-S. Ruetschi, D. Jaccard, M. Gabay, D. A. Muller, J.-M. Triscone, and J. Mannhart, *Science*, **317**, 1196 (2007).

⁵ A. Brinkman, M. Huijben, M. Van Zalk, J. Huijben, U. Zeitler, J. C. Maan, W. G. Van der Wiel, G. Rijnders,

- D. H. A. Blank, and H. Hilgenkamp, *Nature Materials*, **6**, 493 (2007).
- ⁶ A. Kalabukhov, R. Gunnarsson, J. Börjesson, E. Olsson, T. Claeson, and D. Winkler, *Phys. Rev. B*, **75**, 121404 (2007).
- ⁷ W. Siemons, G. Koster, H. Yamamoto, W. A. Harrison, G. Lucovsky, T. H. Geballe, D. H. A. Blank, and M. R. Beasley, *Phys. Rev. Lett.*, **98**, 196802 (2007).
- ⁸ P. R. Willmott, S. A. Pauli, R. Herger, C. M. Schlepütz, D. Martocchia, B. D. Patterson, B. Delley, R. Clarke, D. Kumah, C. Cionca, and Y. Yacoby, *Phys. Rev. Lett.*, **99**, 155502 (2007).
- ⁹ A. S. Kalabukhov, Y. A. Boikov, I. T. Serenkov, V. I. Sakharov, V. N. Popok, R. Gunnarsson, J. Börjesson, N. Ljustina, E. Olsson, D. Winkler, and T. Claeson, *Phys. Rev. Lett.*, **103**, 146101 (2009).
- ¹⁰ L. Qiao, T. C. Droubay, V. Shutthanandan, Z. Zhu, P. V. Sushko, and S. A. Chambers, *Journal of Physics: Condensed Matter*, **22**, 312201 (2010).
- ¹¹ W. Siemons, M. Huijben, G. Rijnders, D. H. A. Blank, T. H. Geballe, M. R. Beasley, and G. Koster, *Phys. Rev. B*, **81**, 241308 (2010).
- ¹² Y. Segal, J. H. Ngai, J. W. Reiner, F. J. Walker, and C. H. Ahn, *Phys. Rev. B*, **80**, 241107 (2009).
- ¹³ W. Siemons, G. Koster, H. Yamamoto, T. H. Geballe, D. H. A. Blank, and M. R. Beasley, *Phys. Rev. B*, **76**, 155111 (2007).
- ¹⁴ K. Yoshimatsu, R. Yasuhara, H. Kumigashira, and M. Oshima, *Phys. Rev. Lett.*, **101**, 026802 (2008).
- ¹⁵ G. Drera, F. Banfi, F. F. Canova, P. Borghetti, L. Sangaletti, F. Bondino, E. Magnano, J. Huijben, M. Huijben, G. Rijnders, D. H. A. Blank, H. Hilgenkamp, and A. Brinkman, *Applied Physics Letters*, **98**, 052907 (2011).
- ¹⁶ S. Chambers, M. Engelhard, V. Shutthanandan, Z. Zhu, T. Droubay, L. Qiao, P. Sushko, T. Feng, H. Lee, T. Gustafsson, E. Garfunkel, A. Shah, J.-M. Zuo, and Q. Ramasse, *Surface Science Reports*, **65**, 317 (2010).
- ¹⁷ G. Koster, B. L. Kropman, G. J. H. M. Rijnders, D. H. A. Blank, and H. Rogalla, *Applied Physics Letters*, **73**, 2920 (1998).
- ¹⁸ V. E. Henrich, G. Dresselhaus, and H. J. Zeiger, *Phys. Rev. B*, **17**, 4908 (1978).
- ¹⁹ R. Courths, B. Cord, and H. Saalfeld, *Solid State Communications*, **70**, 1047 (1989).
- ²⁰ Z. Zhang, S.-P. Jeng, and V. E. Henrich, *Phys. Rev. B*, **43**, 12004 (1991).
- ²¹ K. C. Prince, V. R. Dhanak, P. Finetti, J. F. Walsh, R. Davis, C. A. Muryn, H. S. Dhariwal, G. Thornton, and G. van der Laan, *Phys. Rev. B*, **55**, 9520 (1997).
- ²² Y. Aiura, I. Hase, H. Bando, T. Yasue, T. Saitoh, and D. Dessau, *Surface Science*, **515**, 61 (2002).
- ²³ M. Takizawa, H. Wadati, K. Tanaka, M. Hashimoto, T. Yoshida, A. Fujimori, A. Chikamatsu, H. Kumigashira, M. Oshima, K. Shibuya, T. Mihara, T. Ohnishi, M. Lippmaa, M. Kawasaki, H. Koinuma, S. Okamoto, and A. J. Millis, *Phys. Rev. Lett.*, **97**, 057601 (2006).
- ²⁴ Y. Ishida, R. Eguchi, M. Matsunami, K. Horiba, M. Taguchi, A. Chainani, Y. Senba, H. Ohashi, H. Ohta, and S. Shin, *Phys. Rev. Lett.*, **100**, 056401 (2008).
- ²⁵ E. Stavitski and F. M. de Groot, *Micron*, **41**, 687 (2010).
- ²⁶ T. Higuchi, T. Tsukamoto, N. Sata, M. Ishigame, Y. Tezuka, and S. Shin, *Phys. Rev. B*, **57**, 6978 (1998).
- ²⁷ This procedure neglects doping dependent energy shifts. However, we are interested here in the direct comparison of features of similar origin. ().
- ²⁸ The rescaling factor was calculated according to $I_{OP}/I_{OR} = \exp[-d_{u.c.}/\lambda]$, where $d_{u.c.} = 3.81 \text{ \AA}$ is the dimension of one LaAlO_3 unit cell and $\lambda = 11.3 \text{ \AA}$ is the electron escape length. ().
- ²⁹ T. Fujii, M. Kimura, H. Yoshikawa, and S. Fukushima, *Solid State Communications*, **136**, 375 (2005).
- ³⁰ M. Sing, G. Berner, K. Goß, A. Müller, A. Ruff, A. Wetscherek, S. Thiel, J. Mannhart, S. A. Pauli, C. W. Schneider, P. R. Willmott, M. Gorgoi, F. Schäfers, and R. Claessen, *Phys. Rev. Lett.*, **102**, 176805 (2009).
- ³¹ It is the $\text{La M}_4\text{N}_{4,5}\text{N}_{6,7}$ transition at $E_{kin} = 740 \text{ eV}$ that partly overlaps the Ti 2p emission. S.-J. Oh, G.-H. Kim, G. A. Sawatzky, and H. T. Jonkman, *Phys. Rev. B*, **37**, 6145 (1988).
- ³² S. Tanuma, C. J. Powell, and D. R. Penn, *Surface and Interface Analysis*, **17**, 927 (1991).
- ³³ S. A. Chambers, Y. Liang, Z. Yu, R. Droopad, and J. Ramdani, *J. Vac. Sci. Technol. A*, **19**, 934 (2001).
- ³⁴ Y. Xie, Y. Hikita, C. Bell, and H. Hwang, arXiv, 1105.3891 (2011).
- ³⁵ L. Qiao, T. C. Droubay, T. Varga, M. E. Bowden, V. Shutthanandan, Z. Zhu, T. C. Kaspar, and S. A. Chambers, *Phys. Rev. B*, **83**, 085408 (2011).
- ³⁶ A. Kalabukhov, Y. A. Boikov, I. T. Serenkov, V. I. Sakharov, J. Brjesson, N. Ljustina, E. Olsson, D. Winkler, and T. Claeson, *EPL (Europhysics Letters)*, **93**, 37001 (2011).
- ³⁷ A. Fujimori, I. Hase, M. Nakamura, H. Namatame, Y. Fujishima, Y. Tokura, M. Abbate, F. M. F. de Groot, M. T. Czyzyk, J. C. Fuggle, O. Strebel, F. Lopez, M. Domke, and G. Kaindl, *Phys. Rev. B*, **46**, 9841 (1992).